ISSN 1061-3862, International Journal of Self-Propagating High-Temperature Synthesis, 2017, Vol. 26, No. 1, pp. 33–39. © Allerton Press, Inc., 2017.

FTIR Spectra and Elastic Properties of Cd-Substituted Ni–Zn Ferrites[1]

M. R. Patil[a], M. K. Rendale[b], S. N. Mathad[c,*], and R. B. Pujar[a,d]

[a] *S.S. Arts College and T.P. Science Institute, Sankeshwar, India*

[b] *Department of Engineering Physics, K.L.S. Gogte Institute of Technology, Belagavi, India*

[c] *Department of Engineering Physics, K.L.E. Institute of Technology, Hubli, India*

[d] *Department of Physics, P.C. Jabin Science College, Hubli, India*

**e-mail: physicssiddu@gmail.com*

Received August 2, 2016

Abstract—Solid solutions $Ni_{0.5-x}Cd_xZn_{0.5}Fe_2O_4$ ($x = 0$, 0.15, 0.30) were prepared by solid-state synthesis and characterized by FTIR spectroscopy. The FTIR spectra of synthesized ferrites showed two absorption bands (ν_1 and ν_2) in the range 400–600 cm^{-1} belonging to tetrahedral (A) and octahedral (B) interstitial sites in the spinel lattice. The force constants for tetrahedral (K_t) and octahedral sites (K_o) were determined, as well as Young's modulus (E), rigidity modulus (G), bulk modulus (B), Debye temperature (Θ_D), and velocity of transverse (V_t) and longitudinal (V_l) elastic waves. The relevant interionic cation–anion, cation–cation distances and bond angles are also reported.

Keywords: solid-state synthesis, synthesis by firing, Ni–Zn ferrites, FTIR spectra, elastic modulus, force constants

DOI: 10.3103/S1061386217010083

1. INTRODUCTION

Ferrites deserve attention due to their broad practical application. Ferrite nano particles are the most explored magnetic nano particles up to date. Ferrites are widely used in high-frequency applications, because an AC field does not induce undesirable eddy currents in insulating material [1–3]. The electrical, magnetic, and dielectric properties of ferrite materials depend on their chemical composition, cation distribution, and synthesis procedure. The vibrational, electronic, and magnetic dipole spectra can give information about the position and valence of the ions in the crystal lattice. The FTIR technique shows marked selectivity to chemical composition. Various bands present in IR spectra of ferrites can be regarded as finger prints of characteristic functional groups and bonds [4–7]. The information that can be grabbed from analysis of FTIR spectra is schematically illustrated in Fig. 1. To date, several nanosized ferrites have been fabricated by using solid-state reactions, co-precipitation technique, sol–gel combustion, modified oxidation process, forced hydrolysis, hydrothermal process, ball-milling, aerosol method, and sucrose precursor technique [7–13].

In this communication, we report on detailed FTIR analysis of the $Ni_{0.5-x}Cd_xZn_{0.5}Fe_2O_4$ ($x = 0$, 0.15, 0.30) ferrites prepared by solid-state synthesis.

2. EXPERIMENTAL

High purity nickel oxide, cadmium oxide, zinc oxide, and iron oxide were weighed accurately in required molar proportions and mixed mechanically in an agate mortar in acetone medium. The low-cost solid-state synthesis procedure was essentially the same as reported elsewhere [13]. IR spectra of thick films were recorded in the range 400–750 cm^{-1} with a Perkin Elmer (Spectrum-2000) FTIR spectrophotometer.

3. RESULTS AND DISCUSSIONS

3.1. Structural and Vibrational Analysis

The IR absorption spectra recorded in the range 750–400 cm^{-1} are given in Fig. 2. It is a well-known that normal and inverse cubic spinels have four fundamental IR bands. Two of them, around 600 and 400 cm^{-1}, are common for almost all spinel-type ferrites. In the present work, bands ν_1 and ν_2 were found within the ranges 570–597 and 418–420 cm^{-1}, respectively, and attributed to tetrahedral and octahedral site

[1] The article is published in the original.

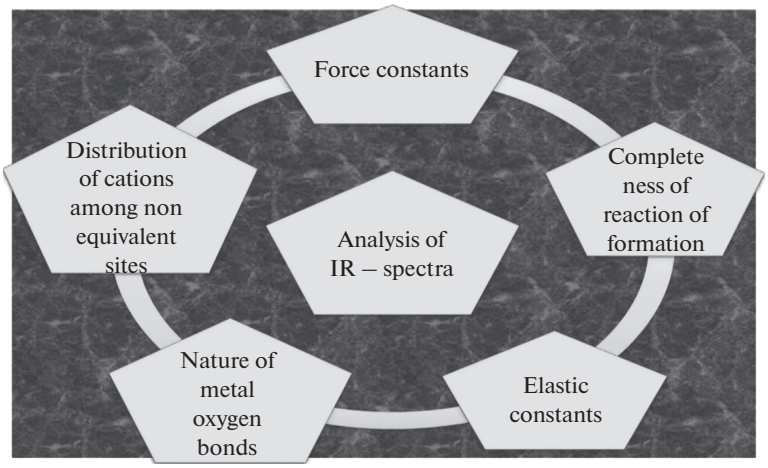

Fig. 1. Information that can be grabbed from analysis of FTIR spectra.

complexes in spinel structure [13, 14]. The IR spectra of Cd-substituted nickel ferrites were found [13] to exhibit two bands in the range 400–700 cm^{-1} but no absorption bands above 700 cm^{-1}.

According to Waldron's classification [4], the unit cell of cubic spinel can be formed by tetrahedral (A) and octahedral (B) sites. Accordingly, band ν_1 can be assigned to stretching vibrations of the tetrahedral metal–oxygen (Me–O) bond while band ν_2, to the metal–oxygen vibrations in octahedral sites. The values of ν_1 are higher than those of ν_2, thus indicating that the normal vibration mode of the tetrahedral complexes is higher than that of the corresponding octahedral sites. This may be due to a shorter bond length in the tetrahedral site compared to that in the octahedral one.

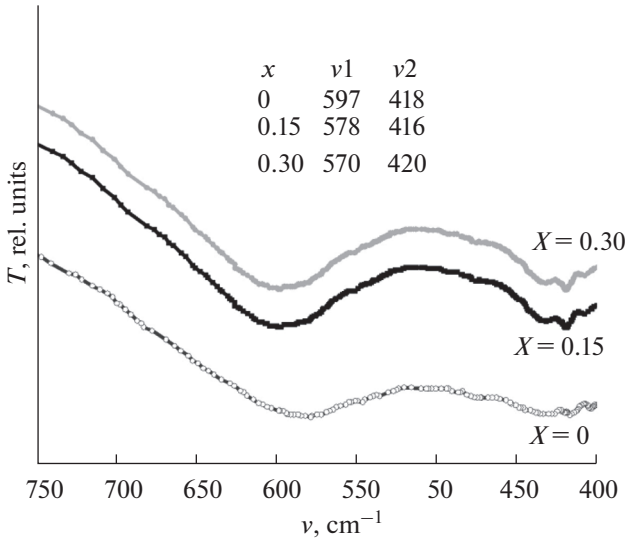

Fig. 2. FTIR spectra of $Ni_{0.5-x}Cd_xZn_{0.5}Fe_2O_4$.

As is known, an increase in site radius reduces the fundamental frequency and therefore the center frequency should shift toward lower values. The increase in site radius may be expected to be due to replacement of smaller Ni^{2+} ions (0.069 nm) by larger Cd^{+2} (0.097 nm) ions. This is due to the fact that substituted Cd^{2+} ions preferentially occupy the A site only and the difference between the ionic radii of A-site Fe^{3+} (0.064 nm) and Cd^{2+} (0.097 nm) cations is much larger as compared to those of B-site Fe^{3+} (0.064 nm) and Ni^{2+} (0.069 nm) cations [14].

Our FTIR spectra show some splitting in the absorption band caused by the presence of small amounts of Fe^{2+} ions in the ferrite. The absorption band edges, as well as tetrahedral (K_t) and octahedral sites (K_0) force constants are given in Table 1.

According to Waldron [4], the force constants are calculated using the following expressions:

$K_0 = 0.942128 M_1 \nu_2^2/[M_A + 32]$, ($M_A$ is molecular weight on A-site)

$K_t = 0.04416 M_B \nu_2^1[V/V + 3]$, ($M_B$ is molecular weight on B-site)

$U = 2K_0/(M_B\nu_1^2 - 2K_0)$, $V = (64 - 2M_AU)/M_B$

Interaction between magnetic moments (μ_B) on lattice sites with regard to the strength of interactions between moments on various sites, the negative interaction or exchange force between the moments of two metal ions on different sites depend on distance between these ions and the oxygen ion that links them and also on the angle between the three ions [15]. The interaction is strongest at an angle of 180° and also where the interatomic distances are shortest. The configuration of ion pairs in spinel ferrites with favorable distances and angles for magnetic interactions are shown in Fig. 3. Interionic distances between the cat-

Table 1. Position of FTIR band edges and force constants for $Ni_{0.5-x}Cd_xZn_{0.5}Fe_2O_4$ ferrites; cation distribution formula: $[Zn_{0.5}Cd_xFe_{0.5-x}]_A[Ni_{0.5-x}Fe_{1.5+x}]_BO_4$

x	Mol. weight, M		Position of band edge, cm^{-1}		Force constants, N/m		
	Site A (M1)	Site B (M2)	ν_1	ν_2	K_t	K_0	K_{av}
0.0	60.62	113.11	597	418	164.63	104.95	134.79
0.15	69.11	112.69	578	416	175.92	103.55	139.73
0.30	77.59	112.26	570	420	192.09	105.15	148.62

ions (Me–Me) (*b*, *c*, *d*, *e*, and *f*) and between the cation and anion (Me–O) (*p*, *q*, *r*, and *s*) were calculated using the measured values of lattice constant (shown in Fig. 3). For A–A and B–B, the angles are too small or the distances between the metal ions (Me) and the oxygen ions (O) are too large. The best combinations of distances and angles are found in the A–B interactions. For an undistorted spinel, the A–O–B angles are about 125 and 154°. The B–O–B angles are 90° and 125° but in the latter, one of the B–O distances is large [15]. In the A–A case, the angle is about 80°. Therefore, the interaction between the moments on the A and B sites is strongest. The B–B interaction is much weaker and the most unfavorable situation occurs in the A–A interaction.

The ferrimagnetism of ferrites is explained on the basis of A–B interaction. An individual A site interacts with a single B site, but each A site is linked to four such units and each B site is linked to six such units [15]. Thus he overall strength of the magnetic interactions (A–B, B–B, and A–A) depends upon the bond length and bond angles between the cations and cation –

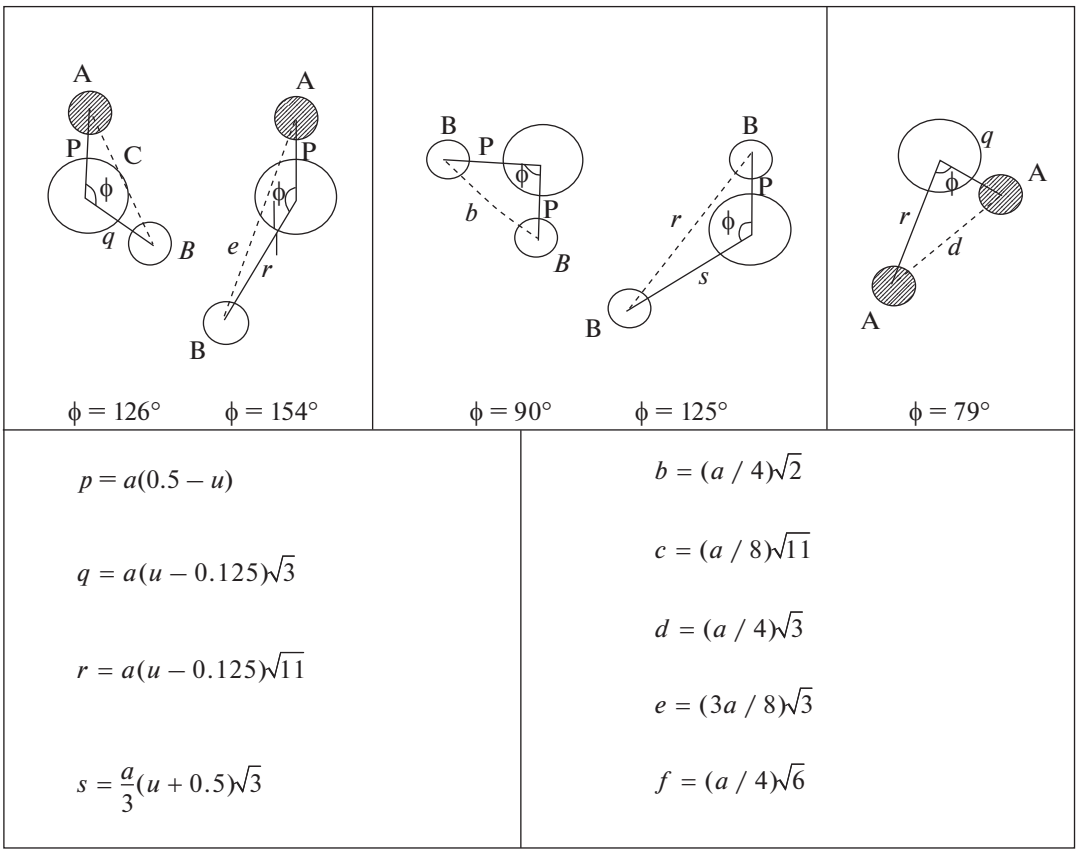

Fig. 3. Interionic distances between Me cations (*b*, *c*, *d*, *e*, and *f*), between Me cation and O anion (*p*, *q*, *r*, and *s*), and bond angles ϕ.

Table 2. Interionic distances (b, c, d, e, f and p, q, r, s) and bond angles (θ)

		$x = 0.0$	$x = 0.15$	$x = 0.30$
Lattice constant a, Å		8.3747	8.4157	8.4600
Me–Me distance, Å	b	2.9609	2.9754	2.9911
	c	3.4720	3.4890	3.5073
	d	3.6264	3.6441	3.6633
	e	5.4395	5.4662	5.4949
	f	5.1284	5.1535	5.1807
Me–O distance, Å	p	1.9681	1.9777	1.9881
	q	2.0308	2.0407	2.0514
	r	3.8886	3.9076	3.9282
	s	3.6989	3.7170	3.7365
Bond angles θ	θ1	120.5	120.5	120.5
	θ_2	133.8	133.8	133.8
	θ_3	97.56	97.56	97.56
	θ_4	126.92	126.92	126.92
	θ_5	67.3	67.3	67.3
Edge and bond lengths	d_{Ax}	1.9176	1.9270	1.9371
	d_{Bx}	0.7033	0.7050	0.7068
	d_{AxE}	3.1315	3.1468	3.1633
	d_{BxE}	2.7904	2.8040	2.8188
	d_{BxEu}	2.9634	2.9779	2.9935

anion. The strength of interaction is directly proportional to bond angle but inversely proportional to bond length.

The bond angles (θ_1, θ_2, θ_3, θ_4 and θ_5) were calculated (see Table 2) by using basic trigonometric principles and the following formulae:

$$\theta_1 = \cos^{-1}\left(\frac{p^2+q^2-c^2}{2pq}\right),\ \theta_2 = \cos^{-1}\left(\frac{p^2+r^2-e^2}{2pr}\right),$$
$$\theta_3 = \cos^{-1}\left(\frac{2p^2-b^2}{2p^2}\right),\ \theta_4 = \cos^{-1}\left(\frac{p^2+s^2-f^2}{2ps}\right),$$
$$\theta_5 = \cos^{-1}\left(\frac{r^2+q^2-d^2}{2rq}\right).$$

The interatomic distances – tetrahedral bond length (d_{Ax}), octahedral bond length (d_{Bx}), shared tetragonal edge (d_{AEx}), shared octahedral edge (d_{BxE}) and unshared octahedral edge (d_{BxEu}) – have been calculated according to [16, 17]:

$$d_{Ax} = a(u - 1/4)\sqrt{3},\ d_{Bx} = a\left(3u^2 - \frac{11}{4}u + \frac{43}{64}\right)^{1/2},$$
$$d_{AxE} = a(2u - \frac{1}{2})\sqrt{2},\ d_{BxE} = a(1-2u)\sqrt{2},$$
$$d_{BxE} = a(1-2u)\sqrt{2},\ d_{BxEu} = a\sqrt{\left(4u^2 - 3u + \frac{11}{16}\right)}.$$

The results are presented in Fig. 4.

3.2. Elastic Properties

Elastic properties of ferrites are of key importance for industrial applications because they define the strength of the materials in different strain conditions. Elastic properties of ferrites can be characterized by FTIR spectroscopy as suggested in [18, 20]. The Debye temperature (Θ_D) is the temperature of crystal's highest normal vibration, i.e., the highest temperature that can be achieved due to a single normal

Table 3. Stiffness constants (C_{11}, B), longitudinal elastic wave (V_l), transverse elastic wave (V_t), mean elastic velocity (V_{av}), rigidity modulus (G), Poisson's ratio (P), Young's modulus (E), and Debye temperature (Θ)

x	C_{11}, GPa	B, GPa	V_l, m/s	V_t, m/s	V_{av}, m/s	G, GPa	P	E, GPa	Θ, K
0.0	160.94	160.94	5480.92	2816.44	2883.63	53.648	0.35	72.425	346.15
0.15	166.04	166.04	5570.25	2862.30	2884.74	55.346	0.35	74.717	344.63
0.30	175.67	175.67	5731.71	2945.18	2885.40	58.557	0.35	79.053	344.34

vibration [18, 19]. Debye temperature simplifies the integration of the heat capacity. For isotropic material, the values of stiffness constants ($C_{11} = C_{12}$), velocity of longitudinal (V_l) and transverse elastic wave (V_t), mean elastic velocity (V_{av}), rigidity modulus (G), Poisson's ratio (P) and Young's modulus (E) were calculated as shown below and collected in Table 3.

$$C_{11} = C_{12} = K_{av}/a,\ V_l = \left(\frac{C_{11}}{dx}\right)^{1/2},\ V_t = \left(V_l/\sqrt{3}\right),$$

$$V_M = \left[V_i^3 V_t^3 / V_t^3 + 2V_i^3\right]^{1/3},\ G = d_x V_t^2,$$

$$B = \frac{1}{3}(C_{11} + 2C_{12}),\ P = \left[\frac{3B - 2G}{6B + 2G}\right],$$

$$E = 2G(1 + P),\ \ \Theta_D = \frac{hcV_{av}}{2\pi k}.$$

A decrease in the values of B, E, and G with increasing x (Table 3) can be interpreted in terms of interatomic bonding [21]. The variation in V_l, V_t, and V_{av} with increasing cadmium content x is plotted in Fig. 5.

An increase in elastic moduli indicates the strengthening of interatomic bonding between various atoms caused by replacement of nickel by cadmium ions as supported by earlier results on variation of elastic moduli with Cd content [14]. The magnitudes of Poisson's ratio (P) were found to be constant (P = 0.35) for all samples, which is consistent with the theory of isotropic elasticity [19]. The elastic parameters and Debye temperature der5ived from IR data well agree with those reported for other ferrite systems [14, 18–22]. Elastic moduli and Debye temperature can be determined through IR spectral analysis and also from increase in elastic constants with increasing x [18, 19]. It should be noted that the values of elastic moduli and Debye temperature determined through ultrasonic pulse transmission technique for Ni–Cd ferrite system synthesized by conventional double sintering ceramic technique showed a decrease with increasing cadmium content.

3.3. Hopping Length

As is seen in Fig. 6, hopping lengths L_A and L_B tend to grow with increasing x. This can be related to expansion of the unit cell caused by an increase in site radius due to embedding larger magnetic Cd^{2+} ions into the B sublattices and migration of nonmagnetic Ni^{2+} ions into the A sublattices, which makes the magnetic ions to approach each other and thus to increase the hopping length. The distance between magnetic ions (hopping length) in tetrahedral A site and octahedral B site were calculated by using the following relations [23]:

$$L_A = \frac{a\sqrt{3}}{4},\ L_B = \frac{a\sqrt{2}}{4},$$

where a stands for the lattice constant.

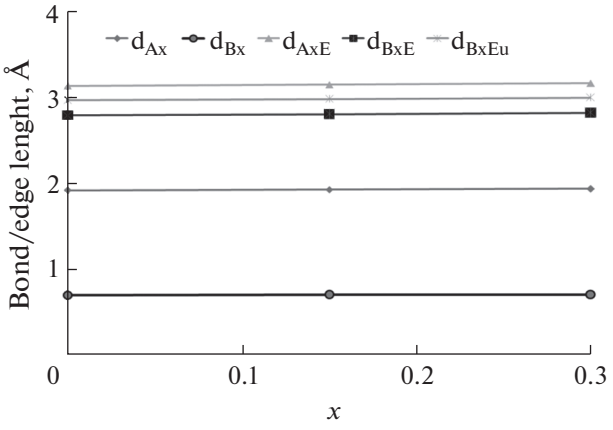

Fig. 4. Bond and edge lengths vs. cadmium content x.

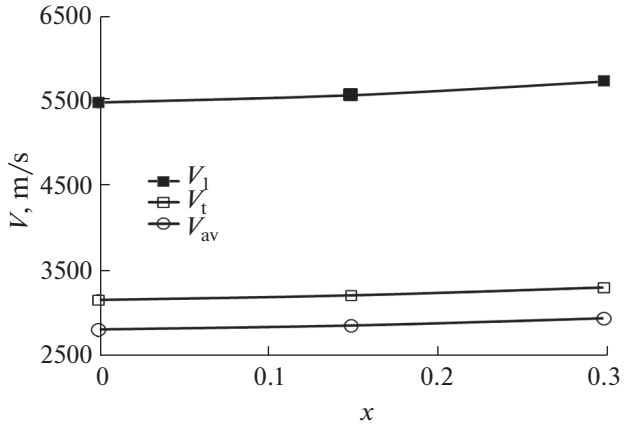

Fig. 5. Variation in velocities of longitudinal (V_l) and transverse (V_t) elastic waves vs. cadmium content x.

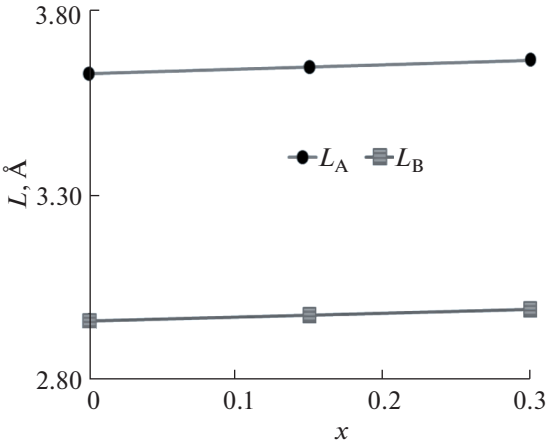

Fig. 6. Hopping lengths L_A and L_B as a function of x.

4. CONCLUSIONS

Analysis of the FTIR spectra of Cd^{+2}-substituted Ni–Zn ferrites reveals a marked increase in the elastic properties of Cd^{+2}-substituted ferrites caused by a larger ionic radius of Cd^{2+} compared to Ni^{2+}. The main absorption bands of spinel ferrites were recorded in the range of 300–700 cm^{-1}. Variation in the elastic properties of ferrites with cadmium content is interpreted in terms of binding forces. Elastic moduli and Debye temperature can be determined through IR spectral analysis and the observed increase in elastic constants with increasing cadmium content is indicative of strengthening the interatomic bonding.

REFERENCES

1. Spaldin, N., *Magnetic Materials: Fundamentals and Device Applications*, Cambridge: Cambridge University Press, 2003. ttp://www.cambridge.org/us/academic/subjects/engineering/magnetic-materials-fundamentals-and-applications-2nd-edition
2. Goldman, A., *Modern Ferrite Technology*, New York: Springer, 2006. http://www.springer.com/la/book/9780387281513
3. Callister, W, *Materials Science and Engineering: An Introduction*, New York: Wiley, 2003.
4. Waldron, R.D., Infrared spectra of ferrites, *Phys. Rev.*, 1953, vol. 99, no. 6, pp. 1727–1735. http://dx.doi.org/doi 10.1103/PhysRev.99.1727
5. Ravinder, D., Far-infrared spectral studies of mixed lithium–zinc ferrites, *Mater. Lett.*, 1999, vol. 40, no. 5, pp. 205–208. dx.doi.org/ doi 10.1016/S0167-577X(99)00075-0
6. Amer, M.A., Ahmed, M.A., El-Nimr, M.K., and Mostafa, M.A., Mössbauer and infrared studies of the Cu–Cr ferrites, *Hyperfine Inter.*, 1995, vol. 96, no. 3, pp. 91–98. doi 10.1007/BF02066275
7. Parmar, V.G., Modi, K.B., and Joshi, H.H., X-ray, SEM, far IR characterization and bulk magnetic properties of Zn^{2+} substituted copper ferrite synthesized by co-precipitation technique, *Indian J. Pure Appl. Phys.*, 1999, vol. 37, no. 3, pp. 207–214. doi nopr.niscair.res.in/bitstream/123456789/27077/1/IJPAP%2037(3)%20207-214.pdf
8. Pradeep Chavan and Naik, L.R., Influence of Ni^{2+} ions on structural, electrical and magnetic properties of magnesium ferrospinels for humidity sensor applications, *Int. J. Eng. Sci. Res.*, 2016, vol. 6, no. 1, pp. 29–42. www.ijesr.org/admin/journal/journal_pradeep%20chavan%20%201feb16esr.pdf
9. Singhal, S., Singh, J., Barthwal, S.K., and Chandra, K., Preparation and characterization of nanosize nickel-substituted cobalt ferrites (CoNiFeO), *J. Solid State Chem.*, 2005, vol. 178, no. 10, pp. 3183–3189. dx.doi.org/ doi 10.1021/jp0039161
10. Sousa, M.H., Tourinho, F.A., Depeyrot, J., da Silva, G.H., and Lara, M.C.F.L., New electric double layered magnetic fluids based on copper nickel, and zinc ferrite nanostructures, *J. Phys. Chem. B*, 2001, vol. 105, no. 6, pp. 1168–1175. dx.doi.org/ doi 10.1016/j.jssc.2005.07.020
11. Yattinahalli, S., Kapatkar, S.B., Ayachit, N.H., and Mathad, S.N., Synthesis and structural characterization of nanosized nickel ferrite, *Int. J. Self-Propag. High-Temp. Synth.*, 2013, vol. 22, no. 3, pp. 147–150. doi 10.3103/S1061386213030114
12. Hanh, N., Quy, O.K., Thuy, N.P., Tung, L.D., and Spinu, L., Synthesis of cobalt ferrite nanocrystallites by forced hydrolysis and investigation of their magnetic properties, *Physica B*, 2003, vol. 327, no. 2, pp. 382–384. dx.doi.org/ doi 10.1016/S0921-4526(02)01750-7
13. Rendale, M.K., Mathad, S.N., and Puri, V., Thick films of magnesium zinc ferrite with lithium substitution: Structural characteristics, *Int. J. Self-Propag. High-Temp. Synth.*, 2015, vol. 24, no. 2, pp. 78–84. doi 10.3103/S1061386215020053
14. Modi, K.B., Rangolia, M.K., Chhantbar, M.C., and Joshi, H.H., Study of infrared spectroscopy and elastic properties of fine and coarse grained nickel–cadmium ferrites, *J. Mater. Sci.*, 2006, vol. 41, no. 22, pp. 7308–7318. doi 10.1007/s10853-006-0929-3

15. Goldman, A., *Modern Ferrite Technology*, ISBN: 978-0-387-28151-3 (print), 978-0-387-29413-1 (online)]. http://www.springer.com/la/book/9780387281513
16. Sharma, R.K., Sebastain, V., Lakshmi, N., Venugopalan, K., Reddy, V.R., and Gupta, A., Variation of structural and hyperfine parameters in nanoparticles of Cr-substituted Co–Zn ferrites, *Phys. Rev. B*, 2007, vol. 75, pp. 144419–144424. http://dx.doi.org/ doi 10.1103/PhysRevB.75.144419
17. Lakhani, V.K., Pathak, T.K., Vasoya, N.H., and Modi, K.B., Structural parameters and X-ray Debye temperature determination study on copper ferrite-aluminates, *Solid State Sci.*, 2011, vol. 13, no. 3, pp. 539–547. http://dx.doi.org/ doi 10.1016/j.solidstatesciences.2010.12.023
18. Modi, K.B., Trivedi, U.N., Pandya, M.P., Bhatu, S.S., Chhantbar, M.C., and Joshi, H.H., Study of elastic properties of magnesium and aluminum co-substituted lithium ferrite near microwave frequencies, in *Microwaves and Optoelectronics*, New Delhi: Anamaya Publishers, 2004, pp. 223–230.
19. Modi, K.B, Elastic moduli determination through IR spectroscopy for zinc substituted copper ferrichromates, *J. Mater. Sci.*, 2004, vol. 39, no. 8, pp. 2887–2890. doi 10.1023/B:JMSC.0000021472.00590.9b
20. Rendale, M.K., Mathad, S.N., and Puri, V., Structural, mechanical and elastic properties of $Ni_{0.7-x}Co_xZn_{0.3}Fe_2O_4$ nanoferrite thick films, *Microelectr. Int.* (in press).
21. Mazen, S.A. and Elmosalami, T.A., IR spectra, elastic, and dielectric properties of Li–Mn ferrite, *Condens. Matter Phys.*, 2012, article ID 907257. http://dx.doi.org/ doi 10.5402/2011/820726
22. Yattinahalli, S.S., Kapatkar, S.B., and Mathad, S.N., Structural and mechanical properties of a nanoferrite, *Adv. Sci. Focus*, 2014, vol. 2, no. 2, pp. 42–46. doi 10.1166/asfo.2014.1079
23. Pathan, A.T., Mathad, S.N., and Shaikh, A.M., Infrared spectral studies of nanostructured Co^{2+}-substituted Li–Ni–Zn ferrites, *Int. J. Self-Propag. High-Temp. Synth.*, 2014, vol. 23, no. 2, pp. 112–117. doi 10.3103/S1061386214020083

SPELL: OK